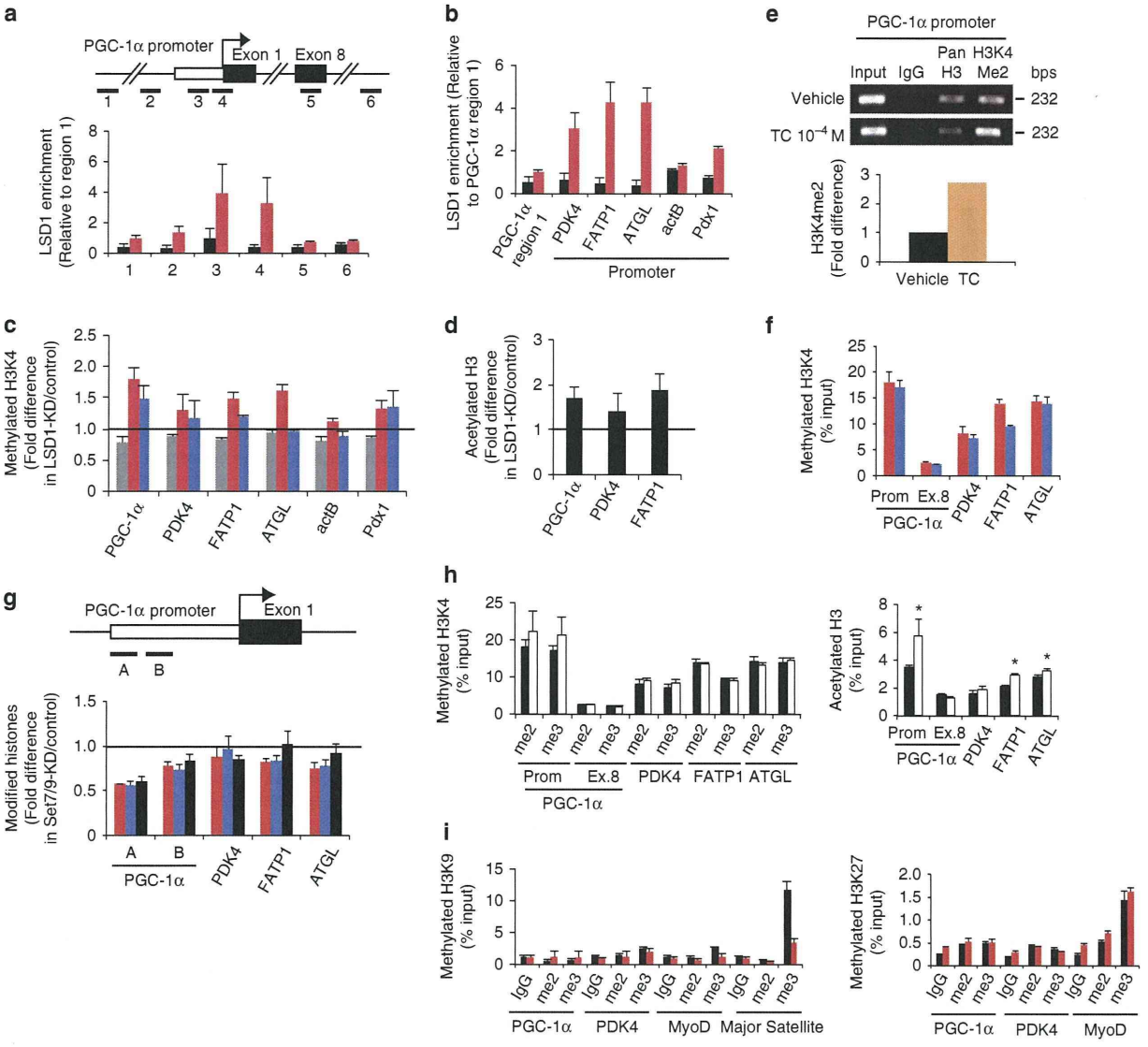

Figure 3 | Epigenetic repression of energy-expenditure genes by LSD1. After 24-hour adipogenic induction, 3T3-L1 cells were examined for LSD1 enrichment and histone modifications by ChIP-qPCR. Before the induction, cells were subjected to siRNA introduction or drug treatment, as specified below. Each ChIP-qPCR histogram indicates the mean±s.d. of triplicate results. (**a**) Localization of LSD1 at the *PGC-1α* gene locus. ChIP analyses were performed in 3T3-L1 cells after 24-hour adipogenic induction using anti-LSD1 antibody. Six indicated sites (1–6) were tested for qPCR amplification. Enrichment values were normalized to input, and shown as the fold difference relative to region 1. Control IgG (black bars), anti-LSD1 antibody (red bars). (**b**) LSD1 occupancy at *PDK4*, *FATP1 ATGL*, *actB* and *Pdx1* gene promoters. LSD1 occupancy was calculated as the enrichment level relative to *PGC-1α* gene exon 8. Control IgG (black bars), anti-LSD1 antibody (red bars). (**c**) ChIP analyses of the target gene promoters using antibodies against mono- (grey bars), di- (red bars) and tri-methylated (blue bars) H3K4. The enrichment values are shown as the fold difference relative to control siRNA-introduced cells. (**d**) Histone H3 acetylation levels of LSD1-target promoters after LSD1-KD. (**e**) Enrichment of di-methylated H3K4 at the *PGC-1α* gene promoter in TC-treated cells. Three independent assays had similar results. (**f**) Di- (red bars) and tri-methylation (blue bars) levels of H3K4 on LSD1-regulated genes. Values indicate percentage of input DNA. (**g**) Histone modification levels of LSD1 target promoters after Set7/9-KD. The enrichment values of di- (red bars), tri- (blue bars) methylated H3K4 and acetylated H3 (black bars) are shown as the fold difference relative to control siRNA-introduced cells. (**h**) Effect of TSA treatment on H3K4 methylation (left panel) and H3 acetylation (right panel). Cells were cultured with vehicle (white bars) or with 100 nM TSA (black bars) before adipogenic induction. *$P < 0.05$ versus vehicle by Student's *t*-test. (**i**) Repressive histone marks in LSD1-KD (red bars) and control (black bars) cells. ChIP experiments were done using antibodies against di- and tri-methylated H3K9 (left panel) and di- and tri-methylated H3K27 (right panel). *MyoD* gene and major satellite repeat were included as experimental controls.

lipid accumulation in differentiating adipocytes (Supplementary Fig. 4c,d). Thus, LSD1 suppresses mitochondrial energy metabolism in mature adipocytes depending on the cellular energy condition.

Because we observed the activated mitochondrial metabolism and the reduced lipid accumulation in LSD1-inhibited states in adipocytes, we checked whether lipolysis was also activated (Fig. 5g,h). Both LSD1-KD and TC treatment in insulin-stimulated mature 3T3-L1 adipocytes significantly augmented the lipolytic activity. Several types of triglyceride lipases are involved in lipolysis and are mainly controlled by the PKA-mediated signal cascade[24,25].

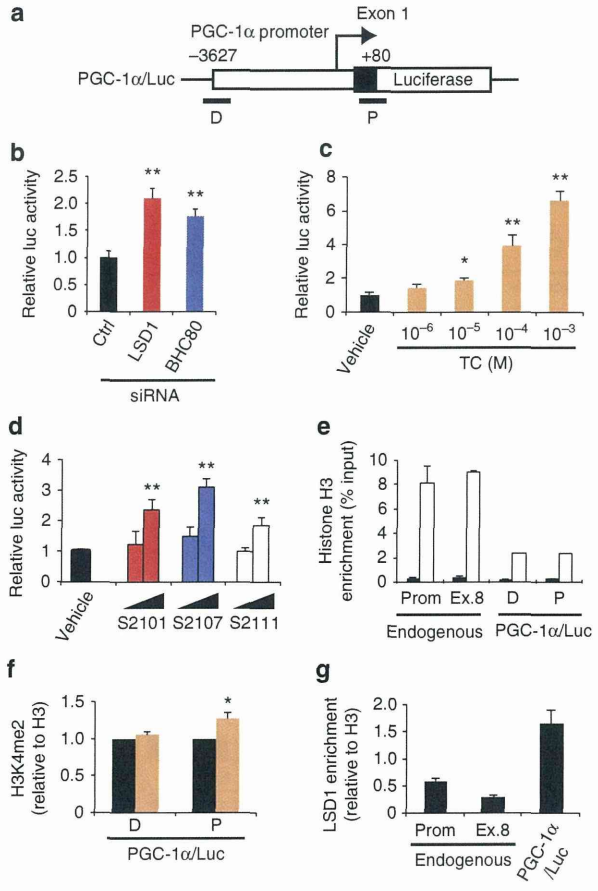

Figure 4 | Transcriptional repression of *PGC-1α* promoter by LSD1. (**a**) Diagram of PGC-1α/Luc construct. Sites of ChIP-qPCR primers are indicated as D (distal) and P (proximal). (**b**) Effects of LSD1-KD and BHC80-KD on *PGC-1α* promoter activity. After the introduction of indicated siRNAs, 3T3-L1 cells were transfected with a PGC-1α/Luc plasmid and an internal control pRL-TK construct. Luciferase activities were measured at 24 h after the adipogenic induction. (**c**,**d**) Effects of LSD1 inhibitors on *PGC-1α* gene promoter activity. TC (**c**) was used at the indicated concentrations whereas SLIs (**d**) were used at 10^{-6} and 10^{-5} M. Reporter-introduced cells were treated with indicated drugs for 24 h before the adipogenic induction. (**e**) Chromatin formation on transfected reporter plasmid. Pan-histone H3 (white bars) and control IgG (black bars) levels were analysed both on endogenous and transgenic *PGC-1α* promoter. (**f**) H3K4 di-methylation level of the reporter vector after vehicle (black bars) or 10^{-4} M TC (orange bars) treatment. Values are normalized to the enrichment level of panH3. (**g**) LSD1-binding on the reporter vector. Values are normalized to the enrichment level of panH3. Values are mean ± s.d. of triplicate samples. $^{*}P < 0.05$, $^{**}P < 0.01$ versus control siRNA or vehicle by Student's *t*-test.

Consistently, *ATGL* and a number of PKA-associated genes were upregulated in *LSD1-inhibited cells* (Fig. 2a–c; Supplementary Data 1). Collectively, these results suggest that LSD1 suppresses energy expenditure by inhibiting mitochondrial respiration and lipid mobilization in adipocytes.

Loss of FAD attenuates the gene regulatory activity of LSD1. To investigate the biological importance of FAD-dependent LSD1 activities, we examined whether cellular FAD synthesis affects the expression of the LSD1-target genes involved in energy metabolism. The biosynthetic pathway from riboflavin to FAD is composed of two enzymes, riboflavin kinase (RFK) and FAD synthetase (FADS)[33] (Fig. 6a). The siRNA-mediated knockdown of these two genes resulted in a mild reduction of the cellular FAD content in 3T3-L1 cells whereas RFK-KD showing the stronger effect, as assessed by two different methods (Supplementary Fig. S5a,b). Expression of most LSD1-target genes was increased by RFK-KD while FADS-KD did not affect *PGC-1α* expression, in agreement with their effects on FAD production (Fig. 6b; Supplementary Fig. S5c). These results imply that RFK is the rate-limiting enzyme in the FAD biosynthetic process. It might be analogous to the case of the NAD^+ (nicotinamide adenine dinucleotide) synthetic pathway in which Nampt, the first enzyme of the process, strongly affects the cellular NAD^+ pool[34]. To elucidate the substantial overlap in the target genes, expression microarray analysis was performed using LSD1-KD and RFK-KD cells (Fig. 6c). A total of 132 genes were commonly induced more than twofold compared with the control under both knockdown conditions. In addition, as we focused on the probe sets upregulated by LSD1-KD, we found significant enrichment of the probe sets that were similarly upregulated by RFK-KD ($P = 3.5 \times 10^{-47}$ by χ^2 test), compared with those oppositely regulated (Fig. 6d).

Earlier studies have identified the 'GxGxxG' sequence as a FAD-binding consensus, one that is frequently present in FAD-dependent oxidases[35] (Supplementary Fig. S5d). To test whether FAD-binding is required for LSD1-mediated transcriptional repression, we point-mutated The 'GxGxxG' motif located at the amino-terminal side to the catalytic domain of LSD1. Structural modelling of LSD1 predicted that these mutations would deteriorate the LSD1/FAD interaction without affecting the overall folding of the protein[36] (Supplementary Fig. S5e,f). In the GAL4 reporter assay, wild-type LSD1 (GAL4-LSD1wt) suppressed the luciferase activities in a dose-dependent manner, whereas FAD binding-defective LSD1 (GAL4-LSD1mut) did not (Fig. 6e). We then tested whether cellular FAD production directly affects the repressive activity of LSD1. When FAD production was impaired by RFK-KD in 3T3-L1 cells, transcriptional repression by GAL4-LSD1wt was partly abolished (Fig. 6f). We also used lumiflavin, a riboflavin analogue that antagonizes the riboflavin transport into the cells[37], which reduced the cellular FAD content (Supplementary Fig. S5g). LSD1 function was abrogated when lumiflavin was added to the culture medium (Fig. 6g). More importantly, the expression of endogenous LSD1 target genes was elevated after lumiflavin treatment (Fig. 6h). Lumiflavin also caused the reduction of LSD1 protein without affecting the messenger RNA level (Supplementary Fig. S5h), raising the possibility that LSD1 protein might be unstable when it is not bound to FAD. Taken together, these results suggest that LSD1 transcriptionally controls energy metabolism in a cellular FAD-dependent manner.

To address whether the metabolic environment affects LSD1 activities, we examined the cellular FAD levels under the lipogenic conditions in 3T3-L1 cells. Interestingly, cellular FAD content remarkably increased during the adipogenic differentiation (Fig. 6i). In addition, palmitate exposure, which has been shown to facilitate lipid storage and suppress PGC-1α expression[38,39], also led to an increase of FAD content in mature 3T3-L1 adipocytes (Fig. 6j). During the adipogenesis, the expression of LSD1-target genes including PGC-1α, PDK4 and FATP1 were increased, possibly reflecting their importance in adipocyte function (Supplementary Fig. S6a). The elevated FAD level may account for the activation of FAD-demanding processes such as fatty acid oxidation and TCA cycle on adipogenic differentiation. Palmitate exposure slightly reduced the expression levels of these genes, although not statistically significant (Supplementary Fig. S6b). The FAD content in the epididymal WAT from normal-diet (ND)- and high-fat-diet (HFD)-fed mice was measured, but no significant difference was found (Supplementary Fig. S6c). In this experiment, FAD concentration was about ten times lower than that of cultured adipocytes, possibly reflecting the

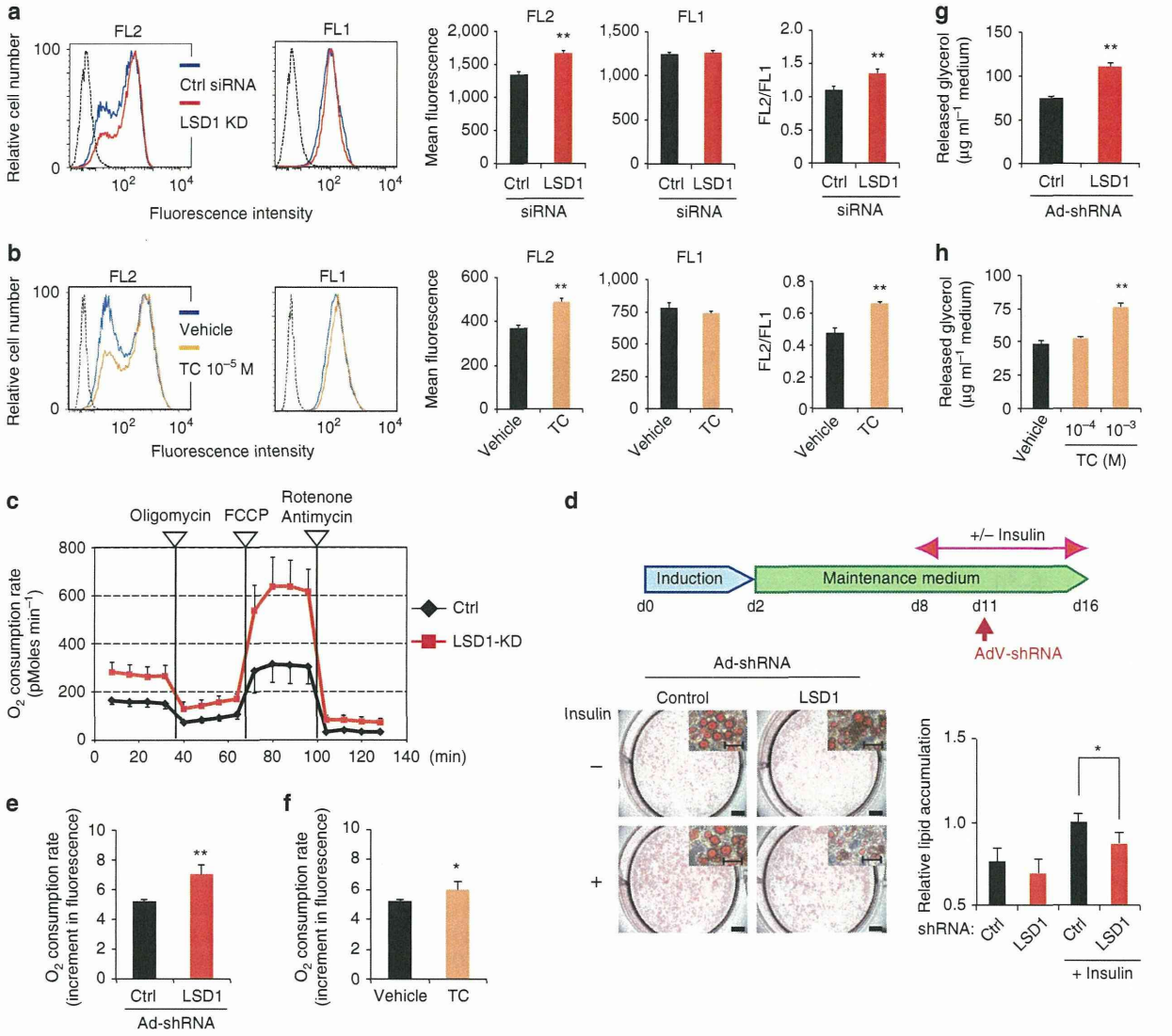

Figure 5 | LSD1 inhibition enhances mitochondrial metabolism in adipocytes. Mitochondrial energy metabolism was assessed in differentiating 3T3-L1 cells under LSD1-KD (**a**) and TC treatment (**b**). siRNA-introduced or drug-treated cells were subjected to adipogenic induction for 24 h, and were stained with JC-1 followed by flow cytometric analyses. Red fluorescent JC-1 aggregates (FL2) and green fluorescent monomers (FL1) were measured. Hatched histograms indicate the unstained control samples. Each histogram shows the representative result of triplicate samples. (**c**) The effect of LSD1-KD on the OXPHOS capacity of differentiating 3T3-L1 cells. OXPHOS activity was determined by measuring the OCR using the XF24 Analyzer. During the real-time measurement, respiratory chain inhibitors were added to the culture at the indicated time points. Values are means±s.d. of five assay wells at each time point. (**d**) LSD1-KD reduces lipid accumulation in insulin-stimulated adipocytes. Differentiated 3T3-L1 cells were cultured in the absence or presence of insulin, followed by adenovirus-mediated introduction of LSD1 shRNA (Ad-shLSD1) or control (Ad-sh-ctrl). Cellular lipid was analysed at 4 days after infection. Values are means±s.d. of five mice. Scale bars in the whole-well and magnified images indicate 5 mm and 50 μm, respectively. (**e**,**f**) The effects of LSD1-KD and TC treatment on the OCR in mature 3T3-L1 adipocytes. Insulin-stimulated adipocytes were treated with shRNA-containing adenoviruses (control or LSD1, **e**) or 10^{-4} M TC (**f**), and cultured for 4 days. OCR was determined using the Oxygen Biosensor System, and was calculated as the fold increase during 30 min-measurement. (**g**,**h**) Enhanced lipolysis in LSD1-inhibited adipocytes. Insulin-stimulated mature 3T3-L1 adipocytes were infected with shRNA-containing adenovirus (**g**) or were treated with TC (**h**), and cultured for 4 days. All values (except for those in **c**) are means±s.d. of three independent samples. $^{*}P<0.05$, $^{**}P<0.01$ versus control siRNA, control shRNA or vehicle by Student's *t*-test

difference in the magnitude of oxidative stress or the instability of FAD in tissue samples. The results show that the FAD content fluctuates depending on the cellular metabolic status, but further study is necessary to elucidate how FAD is utilized in different biological processes in the cell.

Effect of LSD1 inhibition on gene expression in obese WAT. To address the LSD1-dependent metabolic gene regulation *in vivo*, we performed gene-expression analyses in normal and obese adipose tissues of mice. Seven-week old C57BL/6J mice were fed a HFD for six weeks and acquired an obese state. Interestingly, in the adipose tissues of HFD-fed mice, the expression of LSD1 and BHC80 was markedly elevated compared with ND controls (Fig. 7a,b). In addition, the expression of the LSD1 target genes such as *PGC-1α*, *PDK4* and *FATP1* was significantly reduced in the obese WAT tissues (Fig. 7c), indicating an inverse correlation with LSD1/BHC80 expression.

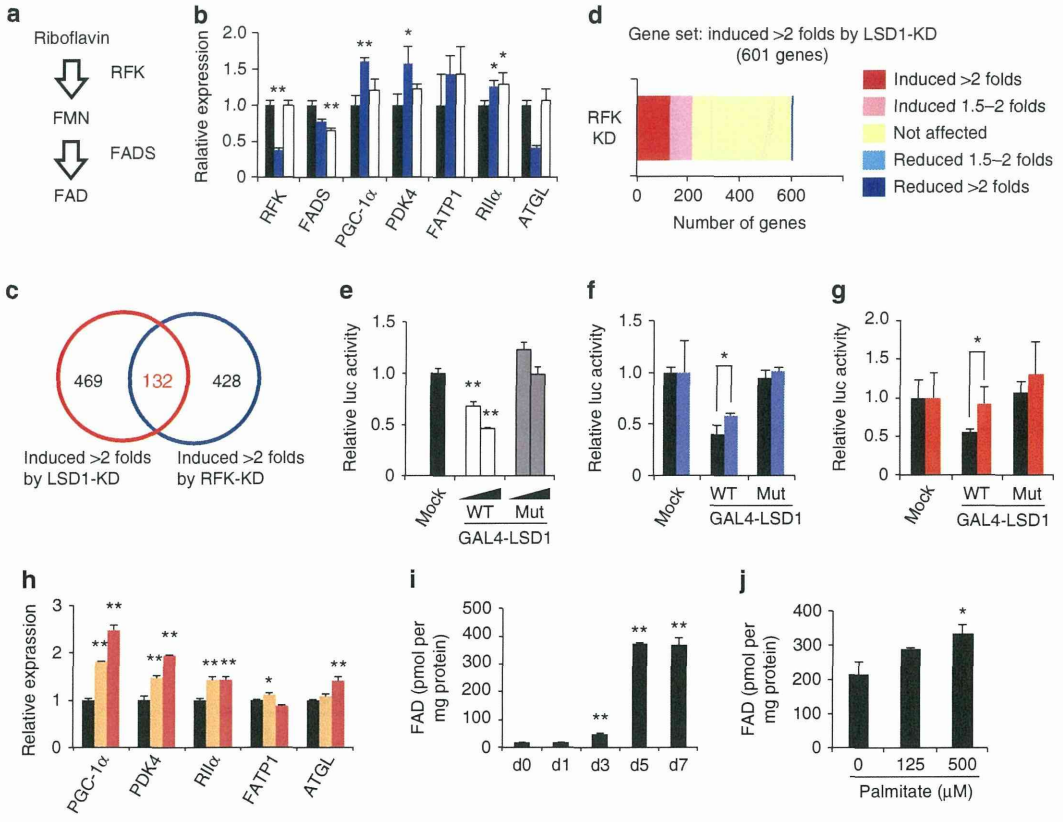

Figure 6 | Inhibition of cellular FAD synthesis blocks LSD1-mediated repression of energy-expenditure genes. (**a**) Biosynthesis pathway of FAD in mammalian cells. Flavin mononucleotide (FMN). (**b**) Effect of the disruption of FAD synthesis on LSD1-target genes. RFK- (blue bars) or FADS- (white bars) knockdown 3T3-L1 cells were induced to differentiate for 24 h, followed by RNA extraction and quantitative RT-PCR. Values are shown as the fold difference against control siRNA-introduced samples (black bars). $^{*}P<0.05$, $^{**}P<0.01$ versus control siRNAs by Student's *t*-test. (**c**) Venn diagram of the probe sets induced by LSD1-KD and RFK-KD. (**d**) Unidirectional effects of RFK-KD on LSD1-target genes. (**e**) Effect of wild-type or FAD-binding mutant-type LSD1 on promoter activity. GAL4-fused LSD1-expressing plasmid (0.1 or 0.5 μg) was transfected into 293T cells, together with the GAL4x5-containing luciferase reporter construct. $^{**}P<0.01$ versus GAL4 mock by Student's *t*-test. (**f**) Effect of RFK-KD on LSD1-mediated transcriptional repression. Control (black bars) or RFK (blue bars) siRNA-introduced 3T3-L1 cells were transfected with indicated GAL4 plasmids 48 h before the luciferase measurement. $^{*}P<0.05$ between indicated conditions by Student's *t*-test. (**g**) Effect of lumiflavin treatment on LSD1-mediated transcriptional repression. 3T3-L1 cells were exposed to vehicle (black bars) or 50 μM lumiflavin (red bars) 48 h before the luciferase measurement. (**h**) Effect of lumiflavin on endogenous LSD1-target genes. Differentiating 3T3-L1 cells were exposed to vehicle (black bars), 25 μM (orange bars) or 50 μM (red bars) lumiflavin for 24 h and were subjected to RNA analyses. (**i**) Increase of FAD concentration during adipogenic differentiation of 3T3-L1 cells. $^{**}P<0.01$ versus day 0 by Student's *t*-test. (**j**) Increase of FAD concentration after 24-hour palmitate exposure in mature 3T3-L1 adipocytes (day 7). Values are normalized to the protein concentration. $^{*}P<0.05$ versus control by Student's *t*-test. All histogram values are means ± s.d. of three independent samples.

To verify the direct relationship between LSD1 function and its target gene expression in obese adipose tissues, we employed the *ex vivo* culture of epididymal WAT in combination with adenovirus-mediated depletion of LSD1. We dissected adipose tissues from HFD-fed obese mice, and analysed the metabolic gene expression, 3 days after adenovirus introduction (at a multiplicity of infection (MOI) of 1.5×10^{8} pfu dissected tissues^{-1}) (Fig. 7d). In agreement with the above data, the loss of LSD1 increased the expression of some energy-expenditure genes such as *PGC-1α* and *PDK4* in obese adipose tissues (Fig. 7e). Interestingly, when tissues from ND-fed mice were used, LSD1-KD did not induce energy-expenditure gene expression suggesting the energetic state-dependent action of LSD1 (Fig. 7f). To further characterize the role of LSD1 in obese adipose tissues *in vivo*, we directly introduced the LSD1 shRNAs-expressing adenovirus into epididymal WAT (at a MOI of 5×10^{8} pfu per mouse). Our repeated experiments using adenoviruses carrying the *EGFP* gene or LSD1 shRNAs showed the efficient introduction of exogenous gene into visceral adipose tissues (Fig. 7g). In agreement with the *ex vivo* studies, LSD1-KD *in vivo* induced relatively small but constant activation of the energy-expenditure genes in obese WAT without any evident tissue/cell defects (Fig. 7h). Thus, LSD1 represses energy-expenditure genes in adipose tissues, possibly participating in the establishment of the metabolic phenotypes *in vivo*.

To evaluate the effect of TC administration on diet-induced obesity and the expression of energy-expenditure genes in adipose tissues *in vivo*, C57BL/6J mice were fed a HFD for six weeks in combination with an alternate-day administration of TC (10 mg per kg body weight) (HFD/TC) or PBS (HFD/PBS). HFD/TC mice showed markedly lower body weight and fat mass compared with the HFD/PBS-mice, with an improvement of the systemic lipid handling (Supplementary Fig. S7a–d). There was no difference in food intake among the groups (Supplementary Fig. S7e), and there were no abnormal behaviour or neurological symptoms in the TC-treated mice. Importantly, TC treatment induced the expression of *PGC-1α* and other LSD1 targets as well as BAT marker *UCP-1* in the epididymal WAT of the HFD/TC mice (Supplementary Fig. S7f).

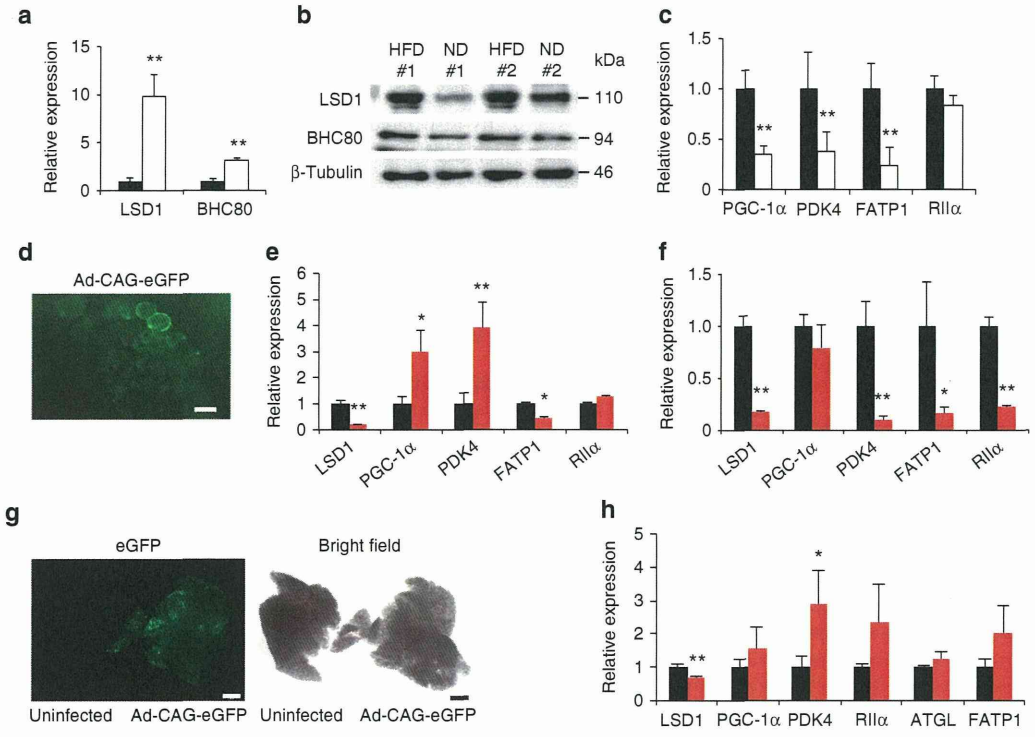

Figure 7 | Inhibition of LSD1 induces energy-expenditure genes in obese adipose tissues. (**a**,**b**) Expression of LSD1 and BHC80 in epididymal WAT from ND (black bars) and HFD- (white bars) fed mice. After a 16-hour fasting period, epididymal WAT was collected, and the total RNA was used for quantitative RT-PCR (**a**). The expression level of the *36B4* gene was used as the internal control. Protein levels are shown by western blot analysis (**b**). (**c**) Expression of LSD1 target genes in ND- (black bars) and HFD- (white bars) fed mice. Values are means±s.d. of four mice, and are shown as fold changes relative to ND-fed mice. $^{**}P<0.01$ versus ND-fed mice by Student's *t*-test. (**d**) Efficient introduction of adenovirus vector into cultured WAT. Adenovirus vector, Ad-CAG-eGFP was introduced into isolated epididymal WAT, and the eGFP expression was analysed by fluorescence microscopy. Scale bar indicates 50 μm. (**e**,**f**) Expression of energy-expenditure genes after adenovirus-mediated knockdown of *LSD1* gene in cultured WAT *ex vivo*. Epididymal WAT was dissected from either HFD- (**e**) or ND-fed mice (**f**), followed by the infection of adenoviruses, Ad-shLSD1 (red bars) or Ad-sh control (black bars). (**g**) Efficient introduction of adenoviral vectors into epididymal WAT *in vivo*. Adenovirus vectors carrying the *eGFP* gene (Ad-CAG-eGFP) was injected into epididymal WAT after incising the outer coat of mice. Four days later, tissues were isolated for the microscopic analysis. Scale bar indicates 2 mm. (**h**) Expression of energy-expenditure genes after adenovirus-mediated reduction of LSD1 in epididymal WAT *in vivo*. Control (black bars) or LSD1 (red bars) shRNA-carrying adenoviruses were directly injected into epididymal WAT of HFD-fed mice 4 days before tissue isolation. Values are means±s.d. of triplicate samples. $^{*}P<0.05$, $^{**}P<0.01$ versus control shRNA by Student's *t*-test.

Collectively, these data further reinforce our finding that LSD1 is involved in the metabolic gene regulation.

Discussion

One of the key factors in formulating an energy strategy is environmental information such as nutritional availability. As many metabolism-associated genes are epigenetically regulated[40], nutrient-driven epigenetic factors may have important roles in forming metabolic phenotypes[3]. LSD1 is a unique demethylase that does not contain the *jumonji* domain but as a flavoenzyme does have the FAD-dependent amine oxidase domain[1]. Our present study clearly indicates that LSD1 negatively regulates energy expenditure that can be reversed by inhibiting LSD1 function and FAD biosynthesis (Fig. 8). Cellular FAD potentiates LSD1 to repress energy-expenditure genes such as *PGC-1α* through H3K4 demethylation in adipocytes where excess energy is stored as triglycerides. Moreover, our experiments using mature adipocytes and isolated adipose tissues revealed the metabolic state-dependent effects of LSD1 inhibition. Thus, the transcriptional and epigenetic regulation by FAD-dependent LSD1 may be central in nutrient-driven metabolic adaptation.

In this study, we identified a set of energy expenditure-associated genes as direct targets of LSD1-mediated repression. We focused on the genes that were commonly induced by LSD1-KD, BHC80-KD and TC treatment. This criterion increased the likelihood of picking up genes that were directly regulated through H3K4 demethylation by LSD1, because BHC80 is reportedly the LSD1 partner required for H3K4 demethylation-dependent repression, and TC irreversibly inhibits the catalytic activity of LSD1 (refs 16,17). This finding was further confirmed by the use of SLIs with minimized nonspecific effects. Our microarray results also revealed the non-overlapping effects of LSD1-KD and BHC80-KD on the genome-wide expression profile. This suggests that in many cases, LSD1 and BHC80 regulate gene expression independently, and that BHC80 is dispensable for LSD1 function other than H3K4 demethylation. In fact, it is reported that BHC80 recognizes H3K4 to facilitate the demethylation by LSD1 (ref. 16), and only a fraction of LSD1 was associated with BHC80 in our experiment (Supplementary Fig. S1c). It is also noteworthy that reported phenotypes of *LSD1*- and *BHC80*-KO mice are distinctively different, indicating the non-overlapping biological function of these genes[11,41].

Mechanistically, LSD1 disruption induced moderate enrichment of methylated H3K4 on actively transcribed promoters. Histone methylation status can be determined by the equilibrium of methylating and demethylating forces, and, in many cases, LSD1 demethylation

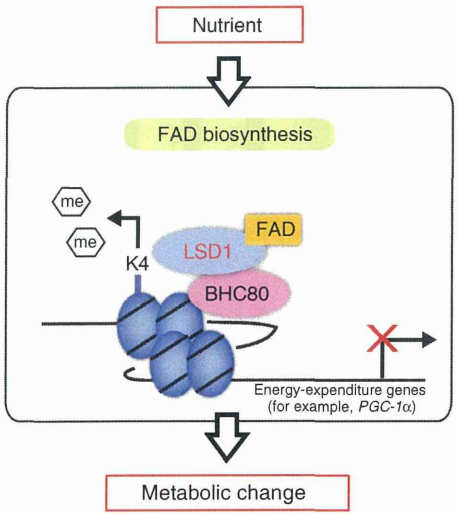

Figure 8 | Schematic model of LSD1 function in the metabolic gene regulation. Schematic model for the epigenetic regulation of energy metabolism by LSD1. FAD-dependent LSD1 facilitates metabolic changes through the repression of energy-expenditure genes via H3K4 demethylation. This pathway may be influenced by nutrients and/or fluctuating FAD level, implicating the link between energetic information and the epigenome.

activity is counteracted by the lysine methyltransferase Set7/9 (refs 9,10). Interestingly, a previous report has shown that glucose-dependent induction of NF-κB gene expression was coincident with Set7/9-dependent H3K4 methylation, and was counteracted by LSD1, implying the possible involvement of Set7/9 in the metabolic gene regulation[42]. In our study, Set7/9-KD resulted in the partial reduction of H3K4 demethylation at LSD1-target promoters (Fig. 3g). Thus, it is possible that LSD1 fine-tunes the expression of metabolic genes so that the cellular energy balance can be properly maintained.

We found in this study that the restriction of cellular FAD availability weakened the LSD1-dependent transcriptional repression of energy-expenditure genes. LSD1, like other flavoenzymes, requires FAD for its catalytic activity and converts it into the reduced form, $FADH_2$ (ref. 43). The catalytic activity of LSD1 may be directly connected to the cellular metabolic state via the fluctuation of the FAD/$FADH_2$ ratio depending on the FAD oxidation processes such as fatty acid β-oxidation and the TCA cycle. Another intriguing possibility is that a physical association between the LSD1 and FAD production machinery determines the LSD1 activities. Indeed, a recent study identified the existence of RFK in the protein complex containing TNFα receptor-1, in which RFK seemed to directly provide NADPH oxidase with FAD, facilitating the TNFα signalling[44]. Such a mechanism might explain why even a small reduction in FAD content in RFK-KD and lumiflavin-treated cells was sufficient for the LSD1 inhibition. In mitochondria, where the majority of FAD production occurs, flavoenzymes may stably associate with FAD even under FAD-reduced conditions[33]. As the FAD reserve for nuclear flavoenzymes is relatively small, their enzymatic activity could be highly sensitive to FAD restriction.

It is of great interest that FAD-dependent LSD1-mediated demethylation may be analogous to, but clearly distinct from, NAD^+-dependent Sirtuin 1 (Sirt1)-mediated deacetylation. Sirt1 is the orthologue of yeast Sir2 histone deacetylase, and promotes mitochondrial activation that contributes to calorie restriction-induced metabolic adaptation[45]. Regarding the regulation of the PGC-1α function, Sirt1 activates PGC-1α protein by deacetylating its lysine residue[46], whereas LSD1 negatively regulates the expression of the *PGC-1α* gene. Such opposing functions of LSD1 and Sirt1 suggest the existence of reciprocal switches for energy homeostasis in which FAD and NAD^+ serve as coenzymatic sensors.

Aberration of cellular energy metabolism is associated with a wide range of multifactor and/or polygenic diseases including obesity-associated diseases, neurological disorders and cancer[47–49]. As epigenetic mechanisms are often linked to the pathogenesis of these diseases, the epigenetic factors responsible would be attractive as pharmacological therapeutic targets[5,50,51]. Our study depicts a novel mechanism of the crosstalk between energy metabolism and epigenetic gene regulation in which the FAD-dependent LSD1 activity regulates energy-expenditure genes. Thus, LSD1 inhibitors may be a new class of epigenetic drugs that can therapeutically benefit a wide range of metabolic disorders.

Methods

Reagents and antibodies. Tranylcypromine hydrochloride, pargyline hydrochloride and lumiflavin were purchased from Sigma. Clorgyline hydrochloride was purchased from MP Biomedicals. The compounds S2101, S2107 and S2111 were synthesized, as previously described[31]. JC-1 was purchased from Molecular Probes. The antibodies used were anti-LSD1 (Abcam, 1:500), anti-mono-methylated histone H3K4 (Abcam, 1:500), anti-di-methylated histone H3K4 (Millipore, 1:500), anti-tri-methylated histone H3K4 (Millipore, 1:500), anti-acetylated histone H3 (Millipore), anti-pan histone H3 (Abcam, 1:2000), anti-di-methylated histone H3K9 (Millipore), anti-tri-methylated histone H3K9 (Millipore), anti-di-methylated histone H3K27 (Millipore), and anti-tri-methylated histone H3K27 (Millipore). Anti-BHC80 antibodies (1:500) were a generous gift from Dr Tadashi Baba (Tsukuba University, Japan)[52]. Antibodies without dilution factors were only used for ChIP experiments. The amount of antibodies used is described here.

Cell culture. Mouse 3T3-L1, C3H10T1/2 cells, and human 293T cells were cultured in DMEM (Sigma) supplemented with 10% (v/v) heat-inactivated fetal bovine serum and penicillin/streptomycin. Adipogenic induction of 3T3-L1 cells was done by a standard method[53]. Post-confluent cells were exposed to adipogenic induction reagents including 0.5 mM 3-isobutyl-1-methylxanthine (Merck), 1 μM dexamethasone (Wako) and 5 μg ml^{-1} insulin (bovine pancreas, Sigma). For the experiments using differentiating adipocytes, cells were collected at 24 h after induction whereas for mature adipocytes, induction medium was replaced with maintenance medium after a 48-h-induction. Lipid accumulation was assessed by oil red O staining. For lipid quantification, oil red O was extracted with 2-propanol and was subjected to colorimetric analysis at 500 nm. For the knockdown experiments, specific siRNAs were introduced to the cells using RNAiMAX reagent (Invitrogen) when they were ~50% confluent. The effective siRNA target sequences are listed in Supplementary Table S3.

Plasmids. To construct pGL3-PGC-1α (PGC-1α/Luc), a luciferase reporter vector containing a mouse *PGC-1α* gene promoter, the fragment (from −3,627 to +80) of this gene was PCR-amplified using primers containing *Mlu*I and *Xho*I sites at the 5′ and 3′ ends, respectively. The GAL4-DNA-binding domain-fused LSD1 expression vector, pcDNA3-GAL4-hLSD1wt, was generated by inserting the *Eco*RI-*Not*I fragment from pcDNA3-Flag-HA-hLSD1 (a gift from Dr Tadashi Baba) into the corresponding sites of pcDNA-GAL4mock. pcDNA3-GAL4-hLSD1mut, which expressed the FAD-binding motif-mutated LSD1, was prepared by site-directed mutagenesis. Two glycine-to-alanine mutations were introduced using the primer pair listed in Supplementary Table S4. GAL4-binding motifs-containing reporter vector (pGL3-GALx5-SNRPN) was described previously[54].

Luciferase reporter assay. Luciferase reporter analyses were performed using a dual-luciferase reporter assay system (Promega), according to the manufacturer's protocol. For *PGC-1α* promoter analysis, the pGL3-PGC-1α reporter vector was co-transfected with the reference vector pRL-TK into 3T3-L1 cells, followed by 24-hour adipogenic induction before luciferase measurement. The siRNAs were introduced 24 h before the reporter transfection. For GAL4 reporter assay, pcDNA-GAL4 plasmids were co-transfected with the reporter plasmid pGL3-GALx5-SNRPN and pRL-TK into 293T or 3T3-L1 cells. After 48-h culture, the cells were collected for luciferase measurement. RFK siRNA was introduced 24 h before plasmid transfection, whereas lumiflavin was added to the culture 24 h before the measurement.

Gene-expression analysis. Total RNA from tissues and cells were extracted using Trizol reagents (Invitrogen). Complementary DNAs were produced using SuperScript III reverse transcriptase (Invitrogen). Quantitative RT–PCR was performed by the SYBR green method using Thunderbird reagents (Toyobo) and ABI 7500 Sequence Detector (Applied Biosciences). Primers used in this study are listed in Supplementary Table S4.

Microarray analysis. Genome-wide expression analysis was performed using a GeneChip Mouse Genome Array 430 2 in combination with a GeneChip

Hybridization, Wash and Stain Kit (Affymetrix). Microarray data were repeatedly confirmed at Takara Dragon Genomics Center (Ohtsu, Japan). siRNA-introduced and TC-treated 3T3-L1 cells were induced to differentiate for 24 h followed by RNA extraction and a quality check using a Bioanalyzer RNA 6000 Nano Assay (Agilent). Data annotation analysis was performed using GeneSpring GX software (Agilent). Gene set enrichment analysis was performed using GSEA ver. 2.0 software provided by the Broad Institute of MIT and Harvard (http://www.broadinstitute.org/gsea/). The accession number of the microarray data in GEO is GSE18600.

Chromatin immunoprecipitation and co-IP. In the ChIP experiments for detecting modified histones, cells were crosslinked with 1% formaldehyde[55]. Following the cell lysis, isolated nuclei were subjected to sonication for chromatin fragmentation. Chromatin fragments were incubated at 4 °C overnight with appropriate antibodies, followed by a pull-down assay using protein A/G-conjugated agarose beads. Purified DNAs were subjected to quantitative PCR (qPCR) using the primer sets listed in Supplementary Table S4. To detect LSD1 enrichment on the genomic DNAs, we employed a protocol for detecting indirect associations between protein and DNA[56]. Briefly, enhanced crosslinking of chromatin using formaldehyde and protein-protein chemical crosslinker DTBP (dimethyl 3, 3′-dithiobispropionimidate 2HCl) (Sigma) was performed to increase the stability of protein-DNA complexes. Chromatin fragmentation was done by sonication in a regular RIPA buffer containing 0.1% SDS, followed by immunoprecipitation, as described above. For co-IP experiments, cells were lysed in IP buffer (50 mM Tris–HCl pH 8.0, 5 mM EDTA 150 mM NaCl, 0.5% NP-40, 0.5% Triton-X100) and incubated with specific antibodies followed by the pull-down with protein A-sepharose beads for subsequent western blot analyses.

Generation of adenoviral vectors that express shRNA. The 65-bp oligonucleotides containing specific shRNA for LSD1 (5′-GATCCCACAAGGAAAGCTA GAAGATTCAAGAGATCTTCTAGCTTTCCTTGTGTTTTTTACGCGTG-3′; the target sequence is underlined), BHC80 (5′-GATCCGTTCCAGATACAGCCATT GTTCAAGAGACAATGGCTGTATCTGGAACTTTTTTACGCGTG-3′) and control GL3 (5′-GATCCGATTTCGAGTCGTCTTAATTTCAAGAGAATTAAGAC GACTCGAAATCTTTTTTACGCGTG-3′) (synthesized by TaKaRa Bio Company) were ligated to the BamHI and EcoRI sites of RNAi-Ready pSIREN-Shuttle Vector (Clontech Laboratories). and were subsequently sequenced for verification. The DNA fragment containing LSD1, BHC80 or GL3-specific shRNA downstream to the human U6 promoter was subcloned into adenoviral vector plasmid pAd.HM4, and was transfected to 293 cells. The generated replication-deficient adenoviral vector was propagated, purified and tittered, as described previously[57,58].

Expression of shRNA in isolated adipose tissues. For *ex vivo* adipose tissue culture, epididymal WAT of mice was obtained, dissected into ~3-mm cubes and maintained in primary culture medium (DMEM/F12 (1:1) supplemented with 10% FBS, 100 μM ascorbic acid, 100 nM insulin and 200 pM 3, 3′, 5-triiodo L-thyronine). For adenovirus infection, three tissue blocks were placed into a single well of 48-well plate and exposed to adenovirus expressing either control or LSD1 shRNA at a MOI of 1.5×10^8 plaque-forming units (pfu) per well. Infections were repeated in triplicate wells for each virus.

***In vivo* introduction of adenoviruses**. We used adenovirus transiently expressing LSD1 shRNAs in WAT *in vivo*, because LSD1-deficient mice and cells had severe defects[11]. For *in vivo* LSD1-knockdown experiments, adenoviruses were directly injected into the epididymal WAT of HFD-fed mice. Under anaesthesia, the outer coats of mice were dissected at the lower part of the abdomen. In obese mice, a portion of epididymal WAT was visible through the peritoneum, enabling targeted injection of adenoviruses. Adenoviruses expressing either control or LSD1 shRNAs were injected into the epididymal WAT on the right side of the abdomen at a MOI of 5×10^8 pfu per mouse. Four days after injection, tissues were collected for RNA analyses.

Assessment of cellular metabolism. For the determination of mitochondrial metabolism, 3T3-L1 cells were stained with fluorescence dye JC-1, followed by flow cytometric analysis[32]. Following trypsinization, cells were exposed to 5 μg ml^{-1} of JC-1 in the culture medium for 15 min at 37 °C and were suspended in PBS for fluorescence-activated cell sorting (FACS) analysis. Green and red fluorescent signals detected mitochondrial mass (FL1) and mitochondrial membrane potential (FL2), respectively, using a FACS Canto cytometer (Becton Dickinson). Cellular lipolytic activity was determined by measuring the concentration of free glycerol released into the culture medium during the 24-h culture, using an Adipolysis Assay Kit (Cayman Chemical). Cellular lactate content was measured using a Lactate Assay Kit II (BioVision), according to the manufacturer's instructions. Oxygen consumption was measured using a BD Oxygen Biosensor (BD Falcon), according to the manufacturer's instructions. For the assay, adipocytes were dispersed into single cells by Accumax reagent (Innovative Cell Technologies) and resuspended in the culture medium. Cell numbers were calculated for the normalization of the oxygen consumption values. Oxygen consumption rate (OCR) values were calculated as the fold-increase during a 30-min-measurement.

Real-time measurement of OXPHOS activity. Real-time monitoring of cellular OXPHOS activity was performed using XF24 Extracellular Flux Analyzer (Seahorse Bioscience), according to the manufacturer's instructions. siRNA-introduced 3T3-L1 cells were inoculated on the assay culture plate and allowed to differentiate for 24 h before the assay. Maximum OXPHOS capacity was determined as previously reported with some modifications[59]. In brief, during the real-time measurement, inhibitors of respiratory chain components were serially added to the culture. First, the complex V inhibitor, oligomycin (1 μg ml^{-1}), was added followed by the addition of the respiratory uncoupler, carbonyl cyanide-*p*-trifluoromethoxyphenylhydrazone (FCCP) (1 μM), and then the complex I and III inhibitors, rotenone (100 nM) and antimycin A (10 μM). After each drug addition, the OCR was measured four times. The addition of FCCP accelerates oxygen consumption to a maximum level, whereas complex I inhibitors completely abolish the mitochondrial respiration. Thus, the difference in OCR between FCCP- and rotenone/antimycin-added states indicates the maximum OXPHOS capacity.

Statistical analyses. Data are presented as means ± s.d. All statistical analyses were performed by a two-tailed Student's *t*-test, except in the microarray experiments, in which Pearson's χ^2 test was carried out.

References

1. Cloos, P. A., Christensen, J., Agger, K. & Helin, K. Erasing the methyl mark: histone demethylases at the center of cellular differentiation and disease. *Genes Dev.* **22,** 1115–1140 (2008).
2. Felsenfeld, G. & Groudine, M. Controlling the double helix. *Nature* **421,** 448–453 (2003).
3. Teperino, R., Schoonjans, K. & Auwerx, J. Histone methyl transferases and demethylases; can they link metabolism and transcription? *Cell Metab.* **12,** 321–327 (2010).
4. Gluckman, P. D. & Hanson, M. A. The developmental origins of the metabolic syndrome. *Trends Endocrinol. Metab.* **15,** 183–187 (2004).
5. Gallou-Kabani, C. & Junien, C. Nutritional epigenomics of metabolic syndrome: new perspective against the epidemic. *Diabetes* **54,** 1899–1906 (2005).
6. Shi, Y. *et al.* Histone demethylation mediated by the nuclear amine oxidase homolog LSD1. *Cell* **119,** 941–953 (2004).
7. Metzger, E. *et al.* LSD1 demethylates repressive histone marks to promote androgen-receptor-dependent transcription. *Nature* **437,** 436–439 (2005).
8. Huang, J. *et al.* p53 is regulated by the lysine demethylase LSD1. *Nature* **449,** 105–108 (2007).
9. Yang, J. *et al.* Reversible methylation of promoter-bound STAT3 by histone-modifying enzymes. *Proc. Natl Acad. Sci. USA* **107,** 21499–21504 (2010).
10. Wang, J. *et al.* The lysine demethylase LSD1 (KDM1) is required for maintenance of global DNA methylation. *Nat. Genet.* **41,** 125–129 (2009).
11. Wang, J. *et al.* Opposing LSD1 complexes function in developmental gene activation and repression programmes. *Nature* **446,** 882–887 (2007).
12. Forneris, F., Binda, C., Vanoni, M. A., Mattevi, A. & Battaglioli, E. Histone demethylation catalysed by LSD1 is a flavin-dependent oxidative process. *FEBS Lett.* **579,** 2203–2207 (2005).
13. Bugg, T. D. H. *Introduction to Enzyme & Coenzyme Chemistry* 2nd edn (Blackwell Publishing, 2004).
14. Modjtahedi, N., Giordanetto, F., Madeo, F. & Kroemer, G. Apoptosis-inducing factor: vital and lethal. *Trends Cell Biol.* **16,** 264–272 (2006).
15. Pospisilik, J. A. *et al.* Targeted deletion of AIF decreases mitochondrial oxidative phosphorylation and protects from obesity and diabetes. *Cell* **131,** 476–491 (2007).
16. Lan, F. *et al.* Recognition of unmethylated histone H3 lysine 4 links BHC80 to LSD1-mediated gene repression. *Nature* **448,** 718–722 (2007).
17. Lee, M. G., Wynder, C., Schmidt, D. M., McCafferty, D. G. & Shiekhattar, R. Histone H3 lysine 4 demethylation is a target of nonselective antidepressive medications. *Chem. Biol.* **13,** 563–567 (2006).
18. Schmidt, D. M. & McCafferty, D. G. trans-2-Phenylcyclopropylamine is a mechanism-based inactivator of the histone demethylase LSD1. *Biochemistry* **46,** 4408–4416 (2007).
19. Gatta, R. & Mantovani, R. NF-Y substitutes H2A-H2B on active cell-cycle promoters: recruitment of CoREST-KDM1 and fine-tuning of H3 methylations. *Nucleic Acids Res,* **36,** 6592–6607 (2008).
20. Zhu, Q. *et al.* Lysine-specific demethylase 1 (LSD1) Is required for the transcriptional repression of the telomerase reverse transcriptase (hTERT) gene. *PLoS One* **3,** e1446 (2008).
21. Jie, Z. *et al.* Trans-2-phenylcyclopropylamine induces nerve cells apoptosis in zebrafish mediated by depression of LSD1 activity. *Brain Res. Bull.* **80,** 79–84 (2009).
22. Youdim, M. B., Edmondson, D. & Tipton, K. F. The therapeutic potential of monoamine oxidase inhibitors. *Nat. Rev. Neurosci.* **7,** 295–309 (2006).
23. Subramanian, A. *et al.* Gene set enrichment analysis: a knowledge-based approach for interpreting genome-wide expression profiles. *Proc. Natl Acad. Sci. USA* **102,** 15545–15550 (2005).

24. Zimmermann, R., Lass, A., Haemmerle, G. & Zechner, R. Fate of fat: the role of adipose triglyceride lipase in lipolysis. *Biochim. Biophys. Acta* **1791,** 494–500 (2009).
25. Holm, C. Molecular mechanisms regulating hormone-sensitive lipase and lipolysis. *Biochem. Soc. Trans.* **31,** 1120–1124 (2003).
26. Sugden, M. C., Bulmer, K. & Holness, M. J. Fuel-sensing mechanisms integrating lipid and carbohydrate utilization. *Biochem. Soc. Trans.* **29,** 272–278 (2001).
27. Puigserver, P. & Spiegelman, B. M. Peroxisome proliferator-activated receptor-gamma coactivator 1 alpha (PGC-1 alpha): transcriptional coactivator and metabolic regulator. *Endocr. Rev.* **24,** 78–90 (2003).
28. Gesta, S., Tseng, Y. H. & Kahn, C. R. Developmental origin of fat: tracking obesity to its source. *Cell* **131,** 242–256 (2007).
29. Wu, Q. *et al.* Fatty acid transport protein 1 is required for nonshivering thermogenesis in brown adipose tissue. *Diabetes* **55,** 3229–3237 (2006).
30. Sebastian, D. *et al.* Novel role of FATP1 in mitochondrial fatty acid oxidation in skeletal muscle cells. *J. Lipid Res.* **50,** 1789–1799 (2009).
31. Mimasu, S. *et al.* Structurally designed trans-2-phenylcyclopropylamine derivatives potently inhibit histone demethylase LSD1/KDM1. *Biochemistry* **49,** 6494–6503 (2010).
32. Lopez-Lluch, G. *et al.* Calorie restriction induces mitochondrial biogenesis and bioenergetic efficiency. *Proc. Natl Acad. Sci. USA* **103,** 1768–1773 (2006).
33. Barile, M., Brizio, C., Valenti, D., De Virgilio, C. & Passarella, S. The riboflavin/FAD cycle in rat liver mitochondria. *Eur. J. Biochem.* **267,** 4888–4900 (2000).
34. Fulco, M. *et al.* Glucose restriction inhibits skeletal myoblast differentiation by activating SIRT1 through AMPK-mediated regulation of Nampt. *Dev. Cell.* **14,** 661–673 (2008).
35. Kubo, A., Itoh, S., Itoh, K. & Kamataki, T. Determination of FAD-binding domain in flavin-containing monooxygenase 1 (FMO1). *Arch. Biochem. Biophys.* **345,** 271–277 (1997).
36. Mimasu, S., Sengoku, T., Fukuzawa, S., Umehara, T. & Yokoyama, S. Crystal structure of histone demethylase LSD1 and tranylcypromine at 2.25 A. *Biochem. Biophys. Res. Commun.* **366,** 15–22 (2008).
37. Bafunno, V. *et al.* Riboflavin uptake and FAD synthesis in Saccharomyces cerevisiae mitochondria: involvement of the Flx1p carrier in FAD export. *J. Biol. Chem.* **279,** 95–102 (2004).
38. Crunkhorn, S. *et al.* Peroxisome proliferator activator receptor gamma coactivator-1 expression is reduced in obesity: potential pathogenic role of saturated fatty acids and p38 mitogen-activated protein kinase activation. *J. Biol. Chem.* **282,** 15439–15450 (2007).
39. Takahashi, K. *et al.* JNK- and IkappaB-dependent pathways regulate MCP-1 but not adiponectin release from artificially hypertrophied 3T3-L1 adipocytes preloaded with palmitate *in vitro*. *Am. J. Physiol. Endocrinol. Metab.* **294,** E898–909 (2008).
40. Gluckman, P. D., Hanson, M. A., Buklijas, T., Low, F. M. & Beedle, A. S. Epigenetic mechanisms that underpin metabolic and cardiovascular diseases. *Nat. Rev. Endocrinol.* **5,** 401–408 (2009).
41. Iwase, S. *et al.* A component of BRAF-HDAC complex, BHC80, is required for neonatal survival in mice. *FEBS Lett.* **580,** 3129–3135 (2006).
42. Brasacchio, D. *et al.* Hyperglycemia induces a dynamic cooperativity of histone methylase and demethylase enzymes associated with gene-activating epigenetic marks that coexist on the lysine tail. *Diabetes* **58,** 1229–1236 (2009).
43. Anand, R. & Marmorstein, R. Structure and mechanism of lysine-specific demethylase enzymes. *J. Biol. Chem.* **282,** 35425–35429 (2007).
44. Yazdanpanah, B. *et al.* Riboflavin kinase couples TNF receptor 1 to NADPH oxidase. *Nature* **460,** 1159–1163 (2009).
45. Lavu, S., Boss, O., Elliott, P. J. & Lambert, P. D. Sirtuins—novel therapeutic targets to treat age-associated diseases. *Nat. Rev. Drug Discov.* **7,** 841–853 (2008).
46. Rodgers, J. T. *et al.* Nutrient control of glucose homeostasis through a complex of PGC-1alpha and SIRT1. *Nature* **434,** 113–118 (2005).
47. Symonds, M. E., Sebert, S. P., Hyatt, M. A. & Budge, H. Nutritional programming of the metabolic syndrome. *Nat. Rev. Endocrinol.* **5,** 604–610 (2009).
48. Knott, A. B., Perkins, G., Schwarzenbacher, R. & Bossy-Wetzel, E. Mitochondrial fragmentation in neurodegeneration. *Nat. Rev. Neurosci.* **9,** 505–518 (2008).
49. DeBerardinis, R. J., Lum, J. J., Hatzivassiliou, G. & Thompson, C. B. The biology of cancer: metabolic reprogramming fuels cell growth and proliferation. *Cell Metab.* **7,** 11–20 (2008).
50. Urdinguio, R. G., Sanchez-Mut, J. V. & Esteller, M. Epigenetic mechanisms in neurological diseases: genes, syndromes, and therapies. *Lancet Neurol.* **8,** 1056–1072 (2009).
51. Kelly, T. K., De Carvalho, D. D. & Jones, P. A. Epigenetic modifications as therapeutic targets. *Nat. Biotechnol.* **28,** 1069–1078 (2010).
52. Iwase, S. *et al.* Characterization of BHC80 in BRAF-HDAC complex, involved in neuron-specific gene repression. *Biochem. Biophys. Res. Commun.* **322,** 601–608 (2004).
53. Okazaki, H. *et al.* Lipolysis in the absence of hormone-sensitive lipase: evidence for a common mechanism regulating distinct lipases. *Diabetes* **51,** 3368–3375 (2002).
54. Fujita, N. *et al.* Mechanism of transcriptional regulation by methyl-CpG binding protein MBD1. *Mol. Cell. Biol.* **20,** 5107–5118 (2000).
55. Ye, S. K. *et al.* The IL-7 receptor controls the accessibility of the TCRgamma locus by Stat5 and histone acetylation. *Immunity* **15,** 813–823 (2001).
56. Fujita, N. *et al.* Methyl-CpG binding domain 1 (MBD1) interacts with the Suv39h1-HP1 heterochromatic complex for DNA methylation-based transcriptional repression. *J. Biol. Chem.* **278,** 24132–24138 (2003).
57. Takahashi, T. *et al.* Identification and isolation of embryonic stem cell-derived target cells by adenoviral conditional targeting. *Mol. Ther.* **14,** 673–683 (2006).
58. Nagano, S., Oshika, H., Fujiwara, H., Komiya, S. & Kosai, K. An efficient construction of conditionally replicating adenoviruses that target tumor cells with multiple factors. *Gene Ther.* **12,** 1385–93 (2005).
59. Hill, B. G., Dranka, B. P., Zou, L., Chatham, J. C. & Darley-Usmar, V. M. Importance of the bioenergetic reserve capacity in response to cardiomyocyte stress induced by 4-hydroxynonenal. *Biochem. J.* **424,** 99–107 (2009).

Acknowledgements

We are grateful to Dr. Tadashi Baba (Tsukuba University, Japan) for kindly providing the plasmids and an antibody. We thank Drs Tatsuya Kondo, Eiichi Araki and Ryuichi Nishinakamura, and Ms. Sayoko Fujimura (Kumamoto University, Japan), and the members of our laboratory for helpful discussions. This work was supported by a Grant-in-Aid for Scientific Research on Priority Areas from the Ministry of Education, Culture, Sports, Science and Technology (M.N. and S.H.), by a Grant-in-Aid for the Global Center of Excellence (COE) 'Cell Fate Regulation Research and Education Unit', Kumamoto University, and by a grant from the Takeda Science Foundation (M.N.).

Author contributions

S.H. and M.N. designed and performed the experiments, together with supports by A.S., K.N. and K.A. Y.W. and K.K. constructed adenovirus vectors. S.M., T.U. and S.Y. synthesized and analysed the small chemicals. S.H., T.U. and M.N. prepared the manuscript.

Additional information

Accession codes: The microarray data have been deposited in the GEO database under accession code GSE18600.

Supplementary Information accompanies this paper at http://www.nature.com/naturecommunications

Competing financial interests: The authors declare no competing financial interests.

Reprints and permission information is available online at http://npg.nature.com/reprintsandpermissions/

How to cite this article: Hino, S. *et al.* FAD-dependent lysine-specific demethylase-1 regulates cellular energy expenditure. *Nat. Commun.* 3:758 doi: 10.1038/ncomms1755 (2012).

THE JOURNAL OF BIOLOGICAL CHEMISTRY VOL. 287, NO. 34, pp. 29101–29113, August 17, 2012

SnoN Suppresses Maturation of Chondrocytes by Mediating Signal Cross-talk between Transforming Growth Factor-β and Bone Morphogenetic Protein Pathways*[S]

Received for publication, February 2, 2012, and in revised form, June 21, 2012 Published, JBC Papers in Press, July 5, 2012, DOI 10.1074/jbc.M112.349415

Ichiro Kawamura[‡§], Shingo Maeda[‡1], Katsuyuki Imamura[‡§], Takao Setoguchi[¶], Masahiro Yokouchi[§], Yasuhiro Ishidou[‡], and Setsuro Komiya[‡§]

From the [‡]Department of Medical Joint Materials, [§]Department of Orthopedic Surgery, and the [¶]Near-Future Locomotor Organ Medicine Creation Course, Graduate School of Medical and Dental Sciences, 8-35-1 Sakuragaoka, Kagoshima University, Kagoshima 890-8544, Japan

Background: BMP signaling promotes chondrocyte maturation and, subsequently, endochondral ossification, whereas TGF-β signaling is inhibitory.
Results: TGF-β induced SnoN to suppress BMP signaling and chondrocyte hypertrophy.
Conclusion: SnoN mediates a signal cross-talk between TGF-β and BMP to regulate chondrocyte maturation.
Significance: Our data revealed an effector of TGF-β signaling as a putative therapeutic molecular target for cartilage/bone regeneration or osteoarthritis.

Hypertrophic maturation of chondrocytes is a crucial step in endochondral ossification, whereas abnormally accelerated differentiation of hypertrophic chondrocytes in articular cartilage is linked to pathogenesis of osteoarthritis. This cellular process is promoted or inhibited by bone morphogenetic protein (BMP) or transforming growth factor-β (TGF-β) signaling, respectively, suggesting that these signaling pathways cross-talk during chondrocyte maturation. Here, we demonstrated that expression of *Tgfb1* was increased, followed by phosphorylation of Smad2, during BMP-2-induced hypertrophic maturation of ATDC5 chondrocytes. Application of a TGF-β type I receptor inhibitor compound, SB431542, increased the expression of *Id1*, without affecting the phosphorylation status of Smad1/5/8, indicating that the activated endogenous TGF-β pathway inhibited BMP signaling downstream of the Smad activation step. We searched for TGF-β-inducible effectors that are able to inhibit BMP signaling in ATDC5 cells and identified SnoN. Overexpression of SnoN suppressed the activity of a BMP-responsive luciferase reporter in COS-7 cells as well as expression of *Id1* in ATDC5 cells and, subsequently, the expression of *Col10a1*, a hallmark of hypertrophic chondrocyte maturation. siRNA-mediated loss of SnoN showed opposite effects in BMP-treated ATDC5 cells. In adult mice, we found the highest level of *SnoN* expression in articular cartilage. Importantly, SnoN was expressed, in combination with phosphorylated Smad2/3, in prehypertrophic chondrocytes in the growth plate of mouse embryo bones and in chondrocytes around the ectopically existing hypertrophic chondrocytes of human osteoarthritis cartilage. Our results indicate that SnoN mediates a negative feedback mechanism evoked by TGF-β to inhibit BMP signaling and, subsequently, hypertrophic maturation of chondrocytes.

Bone formation is achieved by either intramembranous or endochondral ossification. The former process is characterized by differentiation of mesenchymal cells directly into bone-forming osteoblasts. Endochondral ossification is initiated by condensation of mesenchymal cells expressing a chondrogenic master regulator, *Sox9*, after which cells further differentiate into chondrocytes that are able to express a specific marker *Col2a1*, encoding type II collagen (1). Then the committed chondrocytes proliferate and convert into hypertrophic chondrocytes to eventually mineralize the surrounding cartilage matrix to be replaced by bone (2). Hypertrophic chondrocytes are characterized by a round large cell body and the ability to express *Col10a1*, encoding type X collagen. This hypertrophic conversion process is, at least in part, governed by Runx2 protein (*i.e.* Runx2 directly activates the promoter of *Col10a1* to promote chondrocyte hypertrophy) (3, 4). Mouse models in which dominant-negative Runx2 was overexpressed in chondrocytes showed suppressed chondrocyte hypertrophy, combined with complete loss of endochondral ossification (5). Conversely, forced expression of wild-type Runx2 in mouse chondrocytes resulted in accelerated differentiation of hypertrophic chondrocytes and bone formation (5, 6). Given that in permanent cartilage (*e.g.* normal articular cartilage on the joint space), chondrocytes do not undergo the late phase hypertrophic maturation, hypertrophic conversion of chondrocytes must be restricted to maintain a normal cartilage phenotype.

In addition to its indispensable role in physiological bone formation, the endochondral ossification process is a promising cellular event in the application of bone/cartilage regenerative medicine, which can be artificially engineered from human mesenchymal stem/stroma cells (7). Interestingly, these mesenchymal stem/stroma cells form bone trabeculae *in vivo* only

* This work was supported by Grants-in-Aid for Scientific Research (Scientific Research (C) (General)) 23592221 (to S. M.) and 23592222 (to Y. I.) and Japan Orthopedics and Traumatology Foundation, Inc., Grant 254.
[S] This article contains supplemental Table 1 and Fig. 1.
[1] To whom correspondence should be addressed. Tel.: 81-99-275-5381; Fax: 81-99-265-4699; E-mail: s-maeda@m3.kufm.kagoshima-u.ac.jp.

when they have developed hypertrophic structures *in vitro* before implantation (7), indicating that the efficiency of bone regeneration could be improved by promoting hypertrophic maturation of chondrocytes *in vitro*. In the case of cartilage regenerative medicine for treatment of cartilage defects, the maturation processes in engineered chondrocytes must be arrested because abnormally matured hypertrophic chondrocytes, expressing type X collagen, cause pathological conditions (*e.g.* osteoarthritis (OA)[2]) (8–10). *In vitro*, mesenchymal stem/stroma cells rapidly express *COL10A1* in monolayer or pellet culture before the cells demonstrate morphology of hypertrophic chondrocytes, a phenomenon that is a major problem of cartilage tissue engineering (11, 12), suggesting that the mechanism by which mesenchymal stem/stroma cells induce type X collagen is different from that in growth plate chondrocytes. Importantly, it is largely unknown how the expression of type X collagen is induced in degenerating articular chondrocytes.

Both BMP and TGF-β signaling promote early chondrogenesis. Members of the TGF-β family, including BMPs, transduce signals through type II and type I receptors to activate receptor-regulated Smads (R-Smads). Upon ligand binding, TGF-β type I receptors activate Smad2/3, whereas BMP type I receptors phosphorylate Smad1/5/8 in the cytoplasm. After forming a trimeric complex with Smad4 (co-Smad), R-Smads translocate into the nucleus to directly or indirectly regulate the transcription of target genes (13). Forced expression of an extracellular BMP-antagonist, Noggin (*Nog*), in chondrocytes *in vivo* showed no cartilage formation in transgenic mice (14). Similarly, cartilage-specific combined loss of BMP type I receptors (*Bmpr1a* and *Bmpr1b*) or double deletions of BMP-type R-Smads (*Smad1* and *Smad5*) showed severely impaired chondrogenesis in mice (15, 16). These mouse models clearly demonstrated the critical roles of the BMP-Smad pathway in early chondrogenesis. TGF-β signaling promotes the early stage of chondrogenesis by enabling Smad3 to form an active transcriptional complex with CEBP/p300 and Sox9 (17). However, at the late maturation stage, BMP and TGF-β signaling show mutually opposite roles in chondrocyte hypertrophy. BMP signaling directly accelerates the expression of *Col10a1* in concert with Runx2 (18–20), whereas the chondrocyte-specific expression of constitutively active *Bmpr1a* promoted the maturation and hypertrophy of chondrocytes in transgenic mice (21). An intra-articular injection of BMP-2 in mice accelerated cartilage chondrocyte hypertrophy and endochondral ossification to form osteophytes, a phenotype of OA (22). In contrast, loss of TGF-β signaling in the cartilage of mice, achieved by targeted ablation of the *Smad3* gene or forced expression of the dominant negative TGF-β type II receptor, resulted in accelerated differentiation of chondrocytes into hypertrophy coupled with an OA-like destruction of cartilage (23, 24). Similarly, chondrocyte-specific transgenic mice of Smurf2, an E3 ubiquitin ligase of the negative regulator for TGF-β signaling, also showed an OA-like change in articular cartilage with ectopic hypertrophic chondrocytes (25). These mouse models indicated an indispensable role of TGF-β signaling in preventing chondrocyte hypertrophy in articular cartilage, although the underlying molecular mechanisms are unclear. Interestingly, Smad3-deficient chondrocytes showed enhanced BMP signaling and accelerated hypertrophic differentiation *in vitro*, suggesting a role of endogenous TGF-β signaling in suppressing BMP signaling during chondrocyte maturation (26). Taken together, promoting TGF-β signaling in maturing chondrocytes is a promising candidate approach to manipulate the differentiation to fine tune chondrocyte hypertrophy. However, because TGF-β signaling regulates a wide range of pivotal biological functions (*e.g.* cell growth, differentiation, motility, extracellular matrix production, and apoptosis) in various target cells, blocking of the entire TGF-β signaling pathway might result in undesirable side effects. Therefore, to eliminate these problems, the direct mediator(s) induced by TGF-β signaling to inhibit BMP signaling in maturing chondrocytes should be an appropriate molecular target. Here, we show that SnoN is as a spatial and temporal effector of TGF-β signaling to inhibit the BMP-Smad pathway and, subsequently, chondrocyte hypertrophy.

EXPERIMENTAL PROCEDURES

Cell Culture—The chondrogenic cell line ATDC5 was obtained from RIKEN BioResource Center. The cells were maintained in Dulbecco's modified Eagle's medium (DMEM)/Ham's F-12 (1:1) (Invitrogen) containing 5% fetal bovine serum (FBS) and 100 units/ml penicillin G and 100 μg/ml streptomycin. Differentiation of ATDC5 cells was induced in serum-free medium containing insulin/transferrin/selenium supplement (Sigma) on collagen type I-coated culture plates (Iwaki). For expression analysis of differentiation markers in ATDC5 cells, micromass culture was performed as previously described (27), to accelerate maturation of chondrocyte differentiation. A monolayer culture system was employed for analysis of phosphorylation of Smads by immunoblotting because the cell lysis of micromass culture for cytoplasmic/nuclear protein was less efficient, and in addition, these experiments were not intended to evaluate the chondrogenic differentiation of early time points but rather the intracellular signaling. Monolayer culture was also performed for immunocytochemistry because of the difficulty in identifying individual cells in the micromass culture. Primary chondrocytes were harvested from 4-day-old mice of C57BL/6J background as described (28). Primary chondrocytes were induced to differentiate in a monolayer culture. COS-7 cells were purchased from the RIKEN BioResource Center and maintained in DMEM supplemented with 10% FBS and antibiotics.

Ligands and Inhibitors—BMP-2 (Peprotech) was applied at a concentration of 300 ng/ml, whereas TGF-β1 (Peprotech) was used at 5 ng/ml. The day of the first ligand application was referred to as day 0. SB431542 (Sigma) was applied at 1 μM for 30 min prior to ligand stimulation, and DMSO was used as a mock control. When indicated, cells were treated with a proteasome inhibitor, MG132 (Merck), at 10 μM 12 h prior to cell lysis.

Bone Organ Culture—Metatarsal bone rudiments were harvested from C57BL/6J embryos at 17.5 days postcoitum (E17.5) and cultured in DMEM supplemented with 10% FBS, 100

[2] The abbreviations used are: OA, osteoarthritis; BMP, bone morphogenetic protein; qPCR, quantitative PCR; E17.5, embryonic day 17.5.